energies

MDPI

Article

Stannite Quaternary $Cu_2M(M = Ni, Co)SnS_4$ as Low Cost Inorganic Hole Transport Materials in Perovskite Solar Cells

Zohreh Shadrokh [1,*], Shima Sousani [1], Somayeh Gholipour [1], Zahra Dehghani [2], Yaser Abdi [1,*] and Bart Roose [3,*]

[1] Nanophysics Research Laboratory, Department of Physics, University of Tehran, Tehran 1439955961, Iran; sousani.sh68@gmail.com (S.S.); gholipour.somaye@ut.ac.ir (S.G.)

[2] Department of Physics, University of Neyshabur, Neyshabur 9319774400, Iran; Dehghani@neyshabur.ac.ir

[3] Cavendish Laboratory, Department of Physics, University of Cambridge, 19 J. J. Thomson Avenue, Cambridge CB3 0HE, UK

* Correspondence: shadrokh@ut.ac.ir (Z.S.); y.abdi@ut.ac.ir (Y.A.); br340@cam.ac.uk (B.R.)

Received: 20 October 2020; Accepted: 11 November 2020; Published: 13 November 2020

Abstract: In this study, inorganic stannite quaternary $Cu_2M(M = Ni, Co)SnS_4$ (CMTS) is explored as a low-cost, earth abundant, environmentally friendly and chemically stable hole transport material (HTM). CMTS nanoparticles were synthesized via a facile and mild solvothermal method and processed into aggregated nanoparticle inks, which were applied in n-i-p perovskite solar cells (PSCs). The results show that Cu_2NiSnS_4 (CNiTS) is more promising as an HTM than Cu_2CoSnS_4 (CCoTS), showing efficient charge injection as evidenced by considerable photoluminescence quenching and lower series resistance from Nyquist plots, as well as higher power conversion efficiency (PCE). Moreover, the perovskite layer coated by the CMTS HTM showed superior environmental stability after 200 h light soaking in 50% relative humidity, while organic HTMs suffer from a severe drop in perovskite absorption. Although the obtained PCEs are modest, this study shows that the cost effective and stable inorganic CMTSs are promising HTMs, which can contribute towards PSC commercialization, if the field can further optimize CMTS energy levels through compositional engineering.

Keywords: perovskite solar cell; quaternary chalcogenide semiconductor; inorganic hole transport material

1. Introduction

Solar energy is an immensely abundant and clean renewable energy source and one of the most promising technologies to replace fossil fuels. The photovoltaic (PV) market has long been dominated by silicon solar cells, but in the last decade organic-inorganic lead halide perovskite solar cells (PSCs) have gained much ground due to their facile and cost effective solution-based fabrication. A high absorption coefficient [1], and large charge carrier diffusion lengths [2,3] have led to power conversion efficiencies (PCE) > 25% for single junction and >29% for perovskite-silicon tandem solar cells [4], rivalling silicon technology [5–9]. The main obstacle for PSCs towards commercialization now is the long-term device stability [10]. Commonly used hole transport materials (HTMs) have been linked to a number of degradation pathways such as metal migration [11] and degradation of organic components by illumination, temperature and humidity [6,7,9,12,13]. The selection of a suitable HTM will thus be very important in achieving long-term stability of PSCs [14]. HTMs can be divided into organic and inorganic HTMs. Organic HTMs such as 2,2′,7,7′-tetrakis[N,N-di(4-methoxyphenyl)amino]-9,9′-spirobifluorene (spiro-MeOTAD) and poly(triaryl amine) (PTAA), are generally not ideal candidates for commercialization for a number of reasons. Complicated synthesis

processes and the high cost of reactants makes them very costly. Their low intrinsic conductivity means they have to be doped. This not only makes results less reproducible, but many dopants are hygroscopic, attracting moisture that can degrade the perovskite absorber. Low thermal stability (especially of spiro-MeOTAD) means that the HTMs themselves degrade easily and actively contribute to performance loss [9,15–17]. Finally, organic HTMs do not efficiently protect the perovskite absorber layer from the ingress of moisture or metal migration. On the other hand, inorganic HTMs such as NiO_x, CuI, CuSCN, Cu_2O, and $CuInS_2$ are inexpensive, have high intrinsic conductivity, excellent chemical and thermal stability and can protect the perovskite absorber against moisture and metal migration [18–22].

Recently, quaternary chalcogenide Cu-based materials have attracted interest as HTMs for n-i-p and p-i-n PSCs, with a focus on Zn-based materials ($Cu_2ZnSn(S_x,Se_{x-1})_4$ (CZTS)). These materials are low cost, chemically stable, earth-abundant, non-toxic, have a suitable band gap (1.4–1.6 eV) and energy levels, high hole mobility (0.1–35 $cm^2\ V^{-1}\ s^{-1}$) and high absorption coefficient (approximately $10^4\ cm^{-1}$) [23–30]. In this study, Zn is replaced with the magnetic atoms Ni and Co, which form the quaternary stannite-structured Cu_2NiSnS_4 (CNiTS) and Cu_2CoSnS_4 (CCoTS). Their direct and tunable band gap (1.2–1.6 eV), earth-abundant composition, high carrier (hole) mobility (0.36–36 $cm^2\ V^{-1}\ s^{-1}$ for CCoTS, and 3.4–11 $cm^2\ V^{-1}\ s^{-1}$ for CNiTS), thermal stability and high absorption coefficient [31–33], makes them promising HTMs. Thus, we use a solvothermal synthesis approach as it provides a simple and low cost method to synthesize various morphologies and sizes of particles and surface termination by modifying reaction parameters such as time and temperature, capping agents, precursors and solvents [34–37]. We investigate the properties of the CNiTS and CCoTS particles using field-emission scanning electron microscopy (FESEM), X-ray diffraction (XRD) and UV-Vis spectroscopy and utilize photoluminescence (PL) and impedance spectroscopy to assess whether their band energy alignment is suitable for using in PSCs. We find that crystalline CNiTS and CCoTS nano-sheets are formed, where the resulting ink can be utilized as an HTM in n-i-p PSCs. We posit that CNiTS is more suitable as an HTM for PSCs than CCoTS due to better charge transfer may contribute to achieving long-term stability of PSCs. However, the field will have to further optimize the composition of these materials to shift the conduction band upwards and prevent unwanted recombination.

2. Materials and Methods

2.1. Materials

All chemicals were purchased from Merck, unless stated otherwise. Fluorine-doped tin oxide (FTO) glasses (15 Ω^{-1}) and spiro-MeOTAD were purchased from Lumtec, Taiwan (https://www.lumtec.com.tw/).

Lead iodide (PbI_2) and methyl ammonium iodide (MAI) were purchased from Sharif solar, titanium (IV) isopropoxide (TTIP) from Sigma-Aldrich and TiO_2 paste (30 NR-D) was purchased from Greatcell Solar.

2.2. Synthesis of $Cu_2(M = Ni, Co)SnS_4$ (CMTS) Nano-Sheet Particles

The CMTS particles were synthesized by a mild solvothermal method [35]. First, 1 mmol $CuCl_2$, 0.5 mmol $Ni(NO_3)_2{\cdot}6H_2O$ or 0.5 mmol $Co(NO_3)_2{\cdot}6H_2O$, 0.5 mmol $SnCl_2{\cdot}2H_2O$, 2 mmol thiourea, 0.32 g polyvinylpyrrolidone as capping agent and 35 mL ethylene glycol as solvent were stirred for 30 min at 80 °C. The suspension was then transferred into a Teflon container and autoclaved at 180 °C for 8 h. The resulting black suspension was subsequently washed by centrifuging at 9000 rpm with ethanol and deionized (DI) water. The remaining sediment was dried in a vacuum for 12 h at 100 °C (see Figure S1). As can be seen from the XRD pattern of the synthesized CMTS in Figure S2a, tetragonal stannite phases were formed for CNiTS and CCoTS powders. In addition, no secondary phases are found in the Raman spectra (see Figure S2b), which is good evidence of the high purity of the CMTS samples.

2.3. Solar Cell Fabrication

FTO-coated glass substrates were etched using zinc powder and HCl (4 M) to form the electrode pattern. The etching was followed by cleaning in an ultrasonic bath for 15 min using DI water with detergent, acetone, ethanol and isopropanol (IPA). After each step, FTO glasses were rinsed with boiling DI water for several minutes and finally dried with a nitrogen gun. The substrates were kept in a vacuum oven for 2h at 200 °C before use. A TiO_2 blocking layer was spin-coated using a solution of TTIP in ethanol (3000 rpm, 30 s). The substrates were immediately transferred to a hotplate and annealed at 500 °C for 30 min. Next, a mesoporous TiO_2 layer was deposited by spin coating a TiO_2 paste (diluted in ethanol 6:1) (3000 rpm, 30 s) and annealed at 500 °C for 30 min.

PbI_2 films were cast from a 1M solution in *N*,*N*-Dimethylformamide (5000 rpm, 30 s) and annealed at 100 °C for 15 min. The PbI_2 films were then suspended 1 cm above the MAI powder at 150 °C for 3 h in an oven. The resulting $CH_3NH_3PbI_3$ films were washed with IPA to remove excess MAI and dried for 10 min at 150 °C. HTM CMTS powder dispersions (25, 50, 75 100 and 125 $mgmL^{-1}$ in IPA) were spin-coated on the perovskite layer (3000 rpm, 30 s) and annealed for 15 min at 100 °C. An 80 nm layer of Au was deposited on top of the HTM by thermal evaporation to form the back contact.

2.4. Measurements and Characterization

The size and morphology of the CMTS nano-structure particles and perovskite films were characterized by FESEM, (TESCAN, Mira 3-XMU). Structure, crystallinity and the phase of the samples was examined by XRD (D8 Advance Bruker, Cu-Kα λ = 1.54 Å radiation) and by high resolution Raman spectroscopy (SENTERRA, laser wavelength λ = 785 nm, spectral Resolution: <3 cm^{-1}). UV-Vis absorption (Avantes AVASPEC-ULS2048L) was measured in a range from 200 to 1100 nm. Photoluminescence (PL) measurements were performed by using a nitrogen laser (NL 100) with an excitation wavelength of 337 nm.

The current density-voltage (J-V) scans of the PSCs were measured using a solar simulator (Sharif solar, SIM-1000), at a scan rate of 50 mVs^{-1}, under 100 $mWcm^{-2}$ AM 1.5 G illumination, (calibrated using a Thorlabs photodiode). A 0.09 cm^2 mask was used to define the active area. Electrochemical impedance spectroscopy (EIS) measurements were measured under illumination using an Autolab 302 N, at a DC bias potential of 0.8 V and from 10 Hz to 1 MHz. The plots were then fitted using Z-View software.

3. Results

Figure 1a,b shows the solar cell configuration and energy band diagram of the CMTS-based PSCs. As illustrated in Figure 1b, the valence band maximum (VBM) and conduction band minimum (CBM) of CNiTS and CCoTS are at −5.32, −3.87 eV and −5.15, −3.78 eV, respectively [38,39]. This means that the energy levels are well aligned with the VBM and CBM of perovskite to facilitate efficient hole injection at the perovskite/HTM interface, while blocking electrons.

Figure 1c–f shows the top view FESEM images of CNiTS and CCoTS films, which are deposited by 100 mg mL^{-1} ink concentration on the perovskite layer. As can be seen in the FESEM images, aggregated CNiTS and CCoTS nano-sheet particles cover the perovskite surface and form a rough but dense layer. However, some pinholes can be seen (see Figure 1d,f). Different ink concentrations (25, 50, 75, 100 and 125 mg mL^{-1}) were used for solar cell fabrication to optimize the surface coverage and therefore device performance. Further investigations revealed that application of higher ink concentrations results in higher surface coverage. However, vacancies can still be detected even for the highest concentration, which can be attributed to the magnetic properties of Ni and Co, which result in the formation of aggregated and impacted particles (which cannot be separated by sonication). In addition, the choice of ink solvent can affect the surface morphology; nonpolar solvents such as chlorobenzene result in a viscous ink, which does not form a uniform film. On the other hand, for more polar solvents, such as IPA, a uniform film is formed.

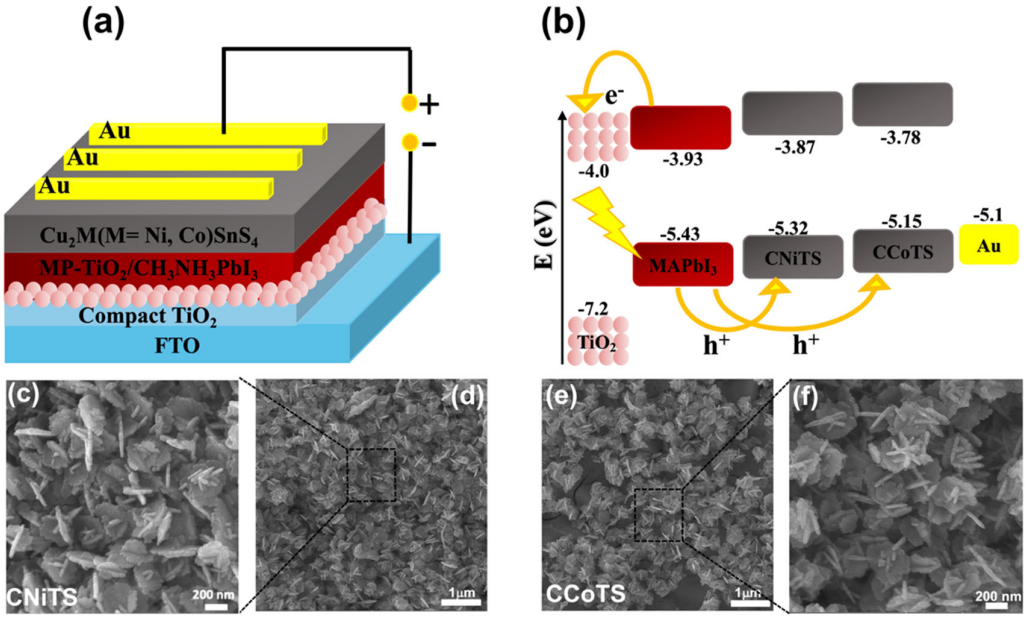

Figure 1. (**a**) Schematic and (**b**) band diagram energy level of perovskite solar cells (PSCs), top-view field-emission scanning electron microscopy (FESEM) images of (**c**), (**d**) Cu_2NiSnS_4 (CNiTS) and (**e**), (**f**) Cu_2CoSnS_4 (CCoTS) layer (deposited by 100 mg mL^{-1} ink concentration for CNiTS and CCoTS) on the perovskite thin film.

The CMTS inks were used to fabricate devices with a FTO/compact-TiO_2/m-TiO_2/$CH_3NH_3PbI_3$/CMTS/Au device configuration. PL and UV-Vis absorption were used to investigate the charge transfer processes. Figure 2a shows the UV-Vis absorption spectra of the CMTS HTMs deposited on top of the perovskite layer. As shown in Figure 2a, the samples exhibit a higher absorption in the visible range (400–800 nm) compared to pristine perovskite; this is attributed to the presence of CMTS. In addition, the presence of CNiTS enhances the absorption considerably more than CCoTS, which may be due to the denser coverage of CNiTS of the perovskite surface (Figure 1c). The UV/Vis absorption spectra of CNiTS and CCoTS are shown in Figure 2b, the corresponding Tauc plots are shown in the inset; an E_g of 1.47 and 1.31 eV is found for CNiTS and CCoTS respectively, which is in agreement with values reported in literature [31,39,40]. Figure 2a also shows the corresponding PL spectra of the CMTS deposited on top of perovskite. The high-intensity PL peak of perovskite at 765 nm will be quenched if charge transfer takes place from the perovskite to the HTM. Quenching is observed for both CNiTS and CCoTS HTMs, but is more pronounced for CNiTS, suggesting charge transfer is more efficient for this material.

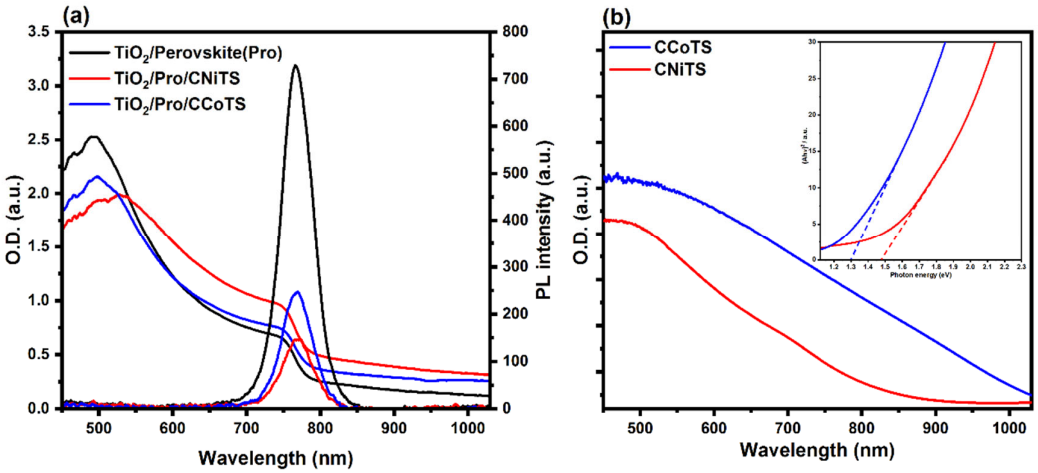

Figure 2. (**a**) UV-Vis absorption and steady photoluminescence (PL) spectra of the FTO/C-TiO_2/M-TiO_2/Perovskite/CMTS film stacks, and (**b**) UV-vis absorption spectra and the Tauc plot (inset) of CM(M = Ni, Co)TS films.

Abbreviations**:** CMTS: $Cu_2M(M = Ni, Co)SnS_4$; FTO: Fluorine-doped tin oxide

In addition, charge transport was studied by EIS, which provides valuable information concerning the interfaces of PSCs. Figure 3a shows the Nyquist plots of the devices with CMTS HTMs. The measurement was carried out under illumination (AM 1.5 G), at 0.8 V bias voltage in a frequency range of 10 Hz to 1 MHz. An equivalent circuit was used to fit the semicircles in Figure 3a containing a series resistance (Rs), charge transfer resistance (Rct) and a constant phase element (CPE) as a nonideal capacitor which is usually defined by CPE-T and CPE-P and is related to the interface capacitor and an ideal capacitor, respectively [23], (see the inset of Figure 3a). The built-in potential is responsible for the interfacial capacitance, which is created by dipoles at the interfaces, thus charge transfer phenomena can be modelled as a constant phase element in parallel with the Rct [41]. The fitted parameters of Rs, Rct, CPE-T, and CPE-P from Nyquist plots are summarized in Table 1. The CPE of the perovskite/CNiTS interface is higher than that of perovskite/CCoTS by 0.5 μF cm^{-2}, which is due to the higher built-in potential (V_{bi}).

The semicircles in Figure 3a can thus be attributed to Rct at the perovskite/HTM interface and the diameter of the arc gives the value for Rct [23,27], which is 211 Ω cm^2 for CNiTS and 264 Ω cm^2 for CCoTS (see Table 1). The smaller Rct of the CNiTS device implies faster charge transport at the perovskite/HTM interface, which is in agreement with the more pronounced quenching of the PL for CNiTS as compared to CCoTS (see Figure 2a).

The intercept on the real Z (Ω cm^2) axis at high frequency corresponds to Rs, which includes the FTO resistance, the intrinsic contact resistance of TiO_2, $CH_3NH_3PbI_3$ and the Au electrode in addition to that of the CMTS HTMs. The Rs of CNiTS is lower than that of CCoTS (20.79 Ω cm^2 and 22.15 Ω cm^2 respectively, Table 1), again suggesting charge injection is more efficient for CNiTS.

Furthermore, on the basis of the characteristic frequency of the Bode-phase plots shown in Figure 3b, the electron lifetime (the recombination time, τ_e) can be calculated by the equation of $\tau_e = 1/2\pi f_{mid}$ (f_{mid} is the phase angle peak at the midfrequency peak). Interestingly, the τ_e value of the CNiTS device (5.8 ms) is higher than that of the CCoTS device (4.9 ms). Again, this further confirms that the perovskite/CNiTS interface has a higher charge lifetime than the perovskite/CCoTS interface.

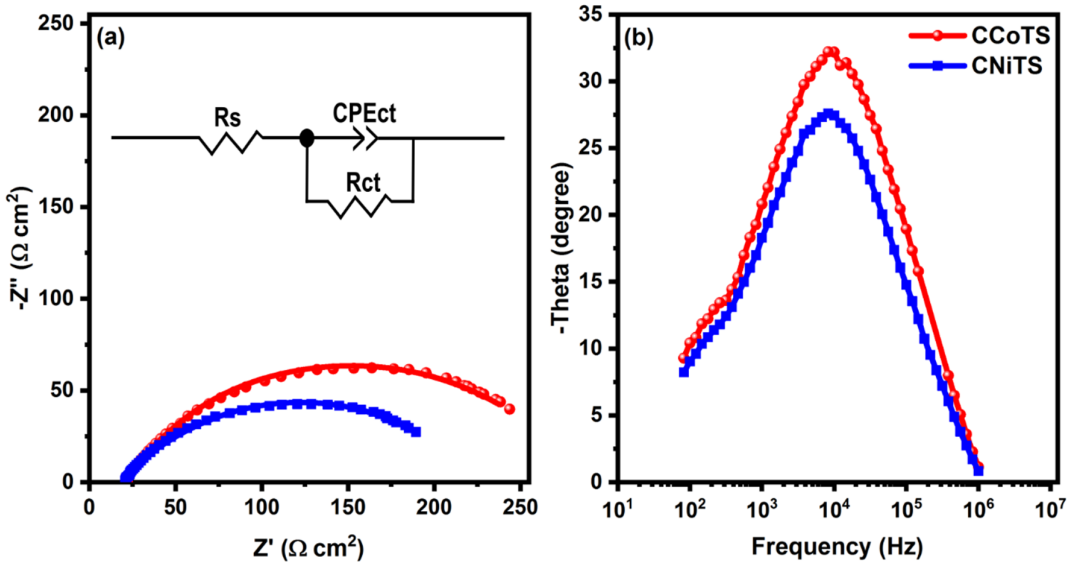

Figure 3. (**a**) Nyquist plots and (**b**) Bode plot of the CM(M = Ni, Co)TS-PSCs under illumination (AM 1.5 G) at the biased voltage of 0.8 V; solid lines show the fitting curves according to equivalent circuit depicted in the inset.

The SEM, PL and EIS data suggest CNiTS will be a more suitable HTM for PSCs than CCoTS. To put this to the test, the concentration of CMTS powder in IPA was optimized to obtain a maximum device performance. The J-V curves of the devices with different CMTS concentrations (25, 50, 75, 100 and 125 mg mL^{-1}) are shown in Figure S3 and the photovoltaic parameters are listed in Table S1. As shown in Table S1, the maximum performance of the PSCs was obtained for a concentration of 100 mg mL^{-1} for both CNiTS and CCoTS. The J-V curves of the CMTS-based PSCs with optimized concentrations of 100 mg mL^{-1} are shown in Figure 4a,b. The obtained photovoltaic parameters from the J-V curves are summarized in Table 1. Dark J-V curves show that shunt resistance is high and series resistance is low for both HTMs, indicating excellent coverage of the perovskite layer and good hole conductivity. The photovoltaic results show a higher performance for CNiTS based-PSCs than that for CCoTS based-PSCs (see Figure S4, for statistical photovoltaic parameters). This may be due to the optimized energy band alignment for CNiTS compared to CCoTS (see Figure 1b) which leads to more efficient charge transport and charge injection [24,26].

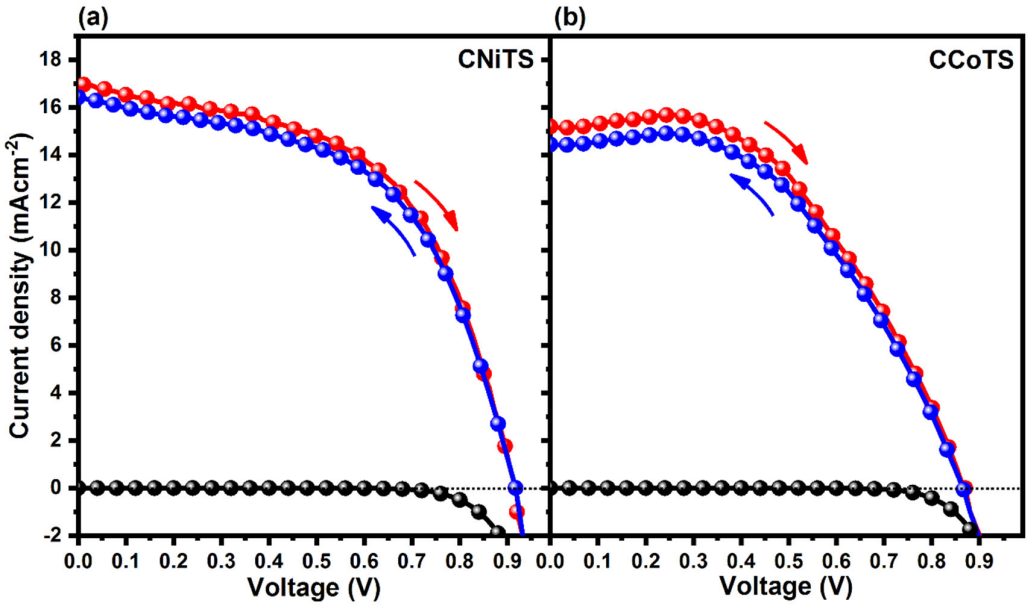

Figure 4. Record current density-voltage (J-V) curves for the (**a**) CNiTS and (**b**) CCoTS-based PSCs, in forward and backward directions with a 50 mVs^{-1} scan rate, under 100 $mWcm^{-2}$ AM 1.5 G illumination and in the dark.

One of the challenges of PSCs is the anomalous hysteresis in the J-V curve, which depends on the scan rate, amplitude of the external electrical field, sweeping direction (from short-circuit towards open-circuit, and vice versa), and architecture of the PSCs [42,43]. It has been shown that hysteresis occurs in the presence of mobile ions and surface defects. The hysteretic behavior of PSCs can thus give information on the quality of the perovskite/HTM interface. Both the devices with CNiTS and CCoTS as HTM demonstrate a small reduction of J_{sc} in the backward scan direction, and no obvious change of V_{oc} and FF. However, the CNiTS HTM shows lower hysteresis (8.5% vs 17.5% for CCoTS), again indicating that CNiTS is more suited as an HTM for PSCs.

However, the obtained PCEs are significantly lower than those reported for state of the art organic HTMs. This may be due to the small offset of the conduction bands of the CMTS HTMs and perovskite, allowing for electron injection into the HTM, leading to significant recombination. In addition, the HTMs are photoactive and may absorb some of the incident light; again this would lead to recombination and reduced device performance. Using compositional engineering (or even quantum confinement) it should be possible to shift the conduction band upwards, as it is in related compounds [44], which would increase hole selectivity and reduce unwanted absorption by the HTM.

Table 1. Photovoltaic parameters of the CM(Ni, Co)TS-based (100 mg mL^{-1}) PSCs with a 50 mVs^{-1} scan rate.

HTM	Scan Direction	V_{oc} (V)	J_{sc} ($mAcm^{-2}$)	FF (%)	PCE (%)	Hysteresis (%)	Rs (Ω cm^2)	Rct (Ω cm^2)	CPE	
									T (F cm^{-2})	Phase
CNiTS	Forward	0.92	17.75	54	8.85	8.5	20.79	211	9×10^{-5}	0.49
	Backward	0.92	16.43	54	8.15					
CCoTS	Forward	0.87	16.87	50	7.31	17.5	22.15	264	4×10^{-5}	0.56
	Backward	0.86	14.45	50	6.22					

We assessed the ability of CCoTS and CNiTS to protect the perovskite absorber layer from environmentally induced degradation by light soaking devices for 200 h in ambient air with 50% relative humidity (see Figure 5). We found that the perovskite absorption is not significantly changed

after light soaking (except around the absorption onset, which is likely caused by light induced trap activation in the perovskite absorber) for both CCoTS and CNiTS. However, the peak absorption at ~500 nm for an equivalent spiro-MeOTAD device shows a ~50% drop. This shows that the inorganic CMTS HTMs are superior when it comes to protecting the perovskite absorber from environmental degradation.

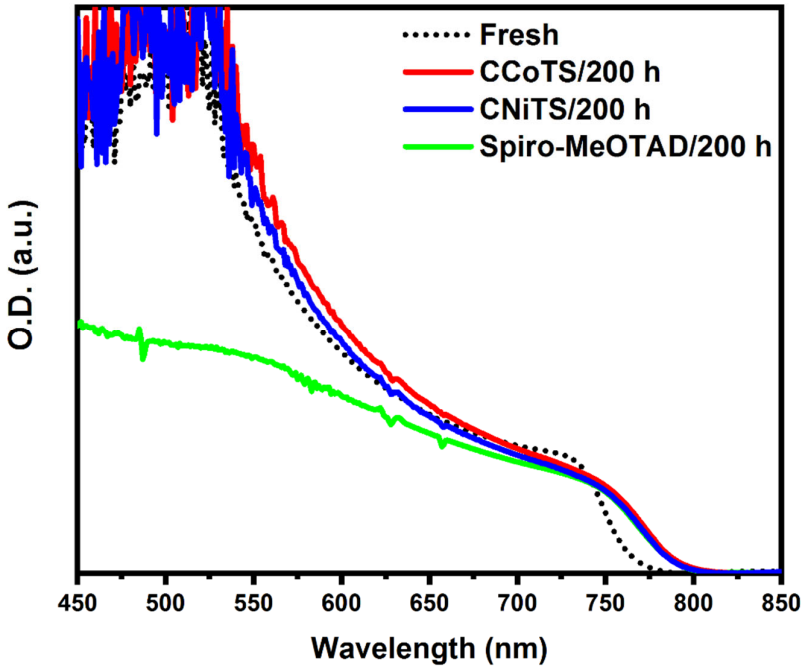

Figure 5. UV-Vis absorption spectra of perovskite-coated CCoTS, CNiTS and spiro-MeOTAD after 200 h of light soaking under AM 1.5 simulated solar light in ambient air (50% relative humidity).

4. Discussion

High purity stannite-structured CMTS particles were synthesized via a cost-effective and facile solvothermal method. Their structural and optical properties were studied to assess their suitability as HTMs for PSCs. Optimized CMTS nano-ink was used in PSCs as an inorganic HTM, which resulted in record PCE of 8.85% for CNiTS and 7.31% for CCoTS. The higher PCE for the CNiTS HTM can be attributed to better charge transfer, which is confirmed by considerable PL quenching and lower charge transport resistance, and by the formation of a more uniform layer on top of perovskite. Moreover, the UV-Vis absorption spectra show that the inorganic CMTS HTMs provide better environmental protection for the perovskite absorber layer, compared to their organic counterparts. We conclude that the quaternary stannite CNiTS is a promising HTM for PSCs, provided that the conduction band can be shifted upwards through compositional engineering. CMTS materials can help pave the way towards stable, low cost and environmentally friendly HTMs and the scalability of PSCs.

Supplementary Materials: The following are available online at www.mdpi.com/1996-1073/13/22/5938/s1, Figure S1: Synthesis process of hole transport materials, Figure S2: X-ray diffraction and Raman spectrum, Figure S3: J-V curves, Figure S4: Statistical photovoltaic parameters, Table S1: Photovoltaic parameters.

Author Contributions: Z.S., S.S., S.G., and Z.D. conceptualized and designed the overall experiments. Z.S. wrote the original draft of the paper. Y.A., and B.R. participated in the supervision of the work. All authors contributed to the discussion and writing of the paper. All authors have read and agreed to the published version of the manuscript.

Funding: This research received no external funding.

Acknowledgments: The authors acknowledge the Iran National Science Foundation and the Royal Society (Newton International Fellowship NF170520) for financial support.

Conflicts of Interest: The authors declare no conflict of interest.

References

1. Im, J.-H.; Lee, C.-R.; Lee, J.-W.; Park, S.-W.; Park, N.-G. 6.5% efficient perovskite quantum-dot-sensitized solar cell. *Nanoscale* **2011**, *3*, 4088–4093, doi:10.1039/C1NR10867K.
2. Stranks, S.D.; Eperon, G.E.; Grancini, G.; Menelaou, C.; Alcocer, M.J.P.; Leijtens, T.; Herz, L.M.; Petrozza, A.; Snaith, H.J. Electron-hole diffusion lengths exceeding 1 micrometer in an organometal trihalide perovskite absorber. *Science* **2013**, *342*, 341–344, doi:10.1126/science.1243982.
3. Dong, Q.; Fang, Y.; Shao, Y.; Mulligan, P.; Qiu, J.; Cao, L.; Huang, J. Electron-hole diffusion lengths > 175 μm in solution-grown CH3NH3PbI3 single crystals. *Science* **2015**, *347*, 967–970, doi:10.1126/science.aaa5760.
4. *Best Research-Cell Efficiency Chart | Photovoltaic Research*; NREL: Golden, CO, USA, 2020.
5. Chopra, K.L.; Paulson, P.D.; Dutta, V. Thin-film solar cells: An overview. *Prog. Photovolt. Res. Appl.* **2004**, *12*, 69–92, doi:10.1002/pip.541.
6. Song, T.-B.; Chen, Q.; Zhou, H.; Jiang, C.; Wang, H.-H.; Yang, Y.; Liu, Y.; You, J.; Yang, Y. Perovskite solar cells: Film formation and properties. *J. Mater. Chem. A* **2015**, *3*, 9032–9050, doi:10.1039/C4TA05246C.
7. Brenner, T.M.; Egger, D.A.; Kronik, L.; Hodes, G.; Cahen, D. Hybrid organic—Inorganic perovskites: Low-cost semiconductors with intriguing charge-transport properties. *Nat. Rev. Mater.* **2016**, *1*, 1–16, doi:10.1038/natrevmats.2015.7.
8. Ibn-Mohammed, T.; Koh, S.C.L.; Reaney, I.M.; Acquaye, A.; Schileo, G.; Mustapha, K.B.; Greenough, R. Perovskite solar cells: An integrated hybrid lifecycle assessment and review in comparison with other photovoltaic technologies. *Renew. Sustain. Energy Rev.* **2017**, *80*, 1321–1344, doi:10.1016/j.rser.2017.05.095.
9. Ko, Y.; Kim, Y.; Lee, C.; Kim, Y.; Jun, Y. Investigation of Hole-Transporting Poly(triarylamine) on Aggregation and Charge Transport for Hysteresisless Scalable Planar Perovskite Solar Cells. *Acs Appl. Mater. Interfaces* **2018**, *10*, 11633–11641, doi:10.1021/acsami.7b18745.
10. Gholipour, S.; Saliba, M. From Exceptional Properties to Stability Challenges of Perovskite Solar Cells. *Small* **2018**, *14*, 1802385, doi:10.1002/smll.201802385.
11. Domanski, K.; Correa-Baena, J.-P.; Mine, N.; Nazeeruddin, M.K.; Abate, A.; Saliba, M.; Tress, W.; Hagfeldt, A.; Grätzel, M. Not All That Glitters Is Gold: Metal-Migration-Induced Degradation in Perovskite Solar Cells. *ACS Nano* **2016**, *10*, 6306–6314, doi:10.1021/acsnano.6b02613.
12. Rosales, B.A.; Hanrahan, M.P.; Boote, B.W.; Rossini, A.J.; Smith, E.A.; Vela, J. Lead Halide Perovskites: Challenges and Opportunities in Advanced Synthesis and Spectroscopy. *ACS Energy Lett.* **2017**, *2*, 906–914, doi:10.1021/acsenergylett.6b00674.
13. Zhang, W.; Eperon, G.E.; Snaith, H.J. Metal halide perovskites for energy applications. *Nat. Energy* **2016**, *1*, 16048, doi:10.1038/nenergy.2016.48.
14. Rajeswari, R.; Mrinalini, M.; Prasanthkumar, S.; Giribabu, L. Emerging of Inorganic Hole Transporting Materials For Perovskite Solar Cells. *Chem. Rec.* **2017**, *17*, 681–699, doi:10.1002/tcr.201600117.
15. Shen, Q.; Ogomi, Y.; Chang, J.; Tsukamoto, S.; Kukihara, K.; Oshima, T.; Osada, N.; Yoshino, K.; Katayama, K.; Toyoda, T.; et al. Charge transfer and recombination at the metal oxide/CH3NH3PbClI2/spiro-OMeTAD interfaces: Uncovering the detailed mechanism behind high efficiency solar cells. *Phys. Chem. Chem. Phys.* **2014**, *16*, 19984–19992, doi:10.1039/C4CP03073G.
16. Kim, G.-W.; Kang, G.; Malekshahi Byranvand, M.; Lee, G.-Y.; Park, T. Gradated Mixed Hole Transport Layer in a Perovskite Solar Cell: Improving Moisture Stability and Efficiency. *ACS Appl. Mater. Interfaces* **2017**, *9*, 27720–27726, doi:10.1021/acsami.7b07071.
17. Adam, G.; Kaltenbrunner, M.; Głowacki, E.D.; Apaydin, D.H.; White, M.S.; Heilbrunner, H.; Tombe, S.; Stadler, P.; Ernecker, B.; Klampfl, C.W.; et al. Solution processed perovskite solar cells using highly conductive PEDOT:PSS interfacial layer. *Sol. Energy Mater. Sol. Cells* **2016**, *157*, 318–325, doi:10.1016/j.solmat.2016.05.011.
18. Cao, J.; Yu, H.; Zhou, S.; Qin, M.; Lau, T.-K.; Lu, X.; Zhao, N.; Wong, C.-P. Low-temperature solution-processed NiOx films for air-stable perovskite solar cells. *J. Mater. Chem. A* **2017**, *5*, 11071–11077, doi:10.1039/C7TA02228J.

19. Zuo, C.; Ding, L. Solution-Processed Cu2O and CuO as Hole Transport Materials for Efficient Perovskite Solar Cells. *Small* **2015**, *11*, 5528–5532, doi:10.1002/smll.201501330.
20. Christians, J.A.; Fung, R.C.M.; Kamat, P.V. An Inorganic Hole Conductor for Organo-Lead Halide Perovskite Solar Cells. Improved Hole Conductivity with Copper Iodide. *J. Am. Chem. Soc.* **2014**, *136*, 758–764, doi:10.1021/ja411014k.
21. Wijeyasinghe, N.; Regoutz, A.; Eisner, F.; Du, T.; Tsetseris, L.; Lin, Y.-H.; Faber, H.; Pattanasattayavong, P.; Li, J.; Yan, F.; et al. Copper(I) Thiocyanate (CuSCN) Hole-Transport Layers Processed from Aqueous Precursor Solutions and Their Application in Thin-Film Transistors and Highly Efficient Organic and Organometal Halide Perovskite Solar Cells. *Adv. Funct. Mater.* **2017**, *27*, 1701818, doi:10.1002/adfm.201701818.
22. Chen, C.; Zhai, Y.; Li, F.; Tan, F.; Yue, G.; Zhang, W.; Wang, M. High efficiency CH3NH3PbI3:CdS perovskite solar cells with CuInS2 as the hole transporting layer. *J. Power Sources* **2017**, *341*, 396–403, doi:10.1016/j.jpowsour.2016.12.027.
23. Wu, Q.; Xue, C.; Li, Y.; Zhou, P.; Liu, W.; Zhu, J.; Dai, S.; Zhu, C.; Yang, S. Kesterite Cu2ZnSnS4 as a Low-Cost Inorganic Hole-Transporting Material for High-Efficiency Perovskite Solar Cells. *ACS Appl. Mater. Interfaces* **2015**, *7*, 28466–28473, doi:10.1021/acsami.5b09572.
24. Cheng, N.; Li, W.; Sun, S.; Zhao, Z.; Xiao, Z.; Sun, Z.; Zi, W.; Fang, L. A simulation study of valence band offset engineering at the perovskite/Cu2ZnSn(Se1-xSx)4 interface for enhanced performance. *Mater. Sci. Semicond. Process.* **2019**, *90*, 59–64, doi:10.1016/j.mssp.2018.10.006.
25. Khanzada, L.S.; Levchuk, I.; Hou, Y.; Azimi, H.; Osvet, A.; Ahmad, R.; Brandl, M.; Herre, P.; Distaso, M.; Hock, R.; et al. Effective Ligand Engineering of the Cu2ZnSnS4 Nanocrystal Surface for Increasing Hole Transport Efficiency in Perovskite Solar Cells. *Adv. Funct. Mater.* **2016**, *26*, 8300–8306, doi:10.1002/adfm.201603441.
26. Yuan, M.; Zhang, X.; Kong, J.; Zhou, W.; Zhou, Z.; Tian, Q.; Meng, Y.; Wu, S.; Kou, D. Controlling the Band Gap to Improve Open-Circuit Voltage in Metal Chalcogenide based Perovskite Solar Cells. *Electrochim. Acta* **2016**, *215*, 374–379, doi:10.1016/j.electacta.2016.08.130.
27. Patel, S.B.; Patel, A.H.; Gohel, J.V. A novel and cost effective CZTS hole transport material applied in perovskite solar cells. *CrystEngComm* **2018**, *20*, 7677–7687, doi:10.1039/C8CE01337C.
28. Ashebir, G.Y.; Dong, C.; Wan, Z.; Qi, J.; Chen, J.; Zhao, Q.; Chen, W.; Wang, M. Solution-processed Cu2ZnSnS4 nanoparticle film as efficient hole transporting layer for stable perovskite solar cells. *J. Phys. Chem. Solids* **2019**, *129*, 204–208, doi:10.1016/j.jpcs.2019.01.008.
29. Zhuk, S.; Kushwaha, A.; Wong, T.K.S.; Masudy-Panah, S.; Smirnov, A.; Dalapati, G.K. Critical review on sputter-deposited Cu2ZnSnS4 (CZTS) based thin film photovoltaic technology focusing on device architecture and absorber quality on the solar cells performance. *Sol. Energy Mater. Sol. Cells* **2017**, *171*, 239–252, doi:10.1016/j.solmat.2017.05.064.
30. Hages, C.J.; Agrawal, R. Synthesis of CZTSSe Thin Films from Nanocrystal Inks. In *Copper Zinc Tin Sulfide-Based Thin-Film Solar Cells*; John Wiley & Sons, Ltd.: Hoboken, NJ, USA, 2015; pp. 239–270, ISBN 978-1-118-43786-5.
31. Krishnaiah, M.; Bhargava, P.; Mallick, S. Low-temperature synthesis of Cu2CoSnS4 nanoparticles by thermal decomposition of metal precursors and the study of its structural, optical and electrical properties for photovoltaic applications. *RSC Adv.* **2015**, *5*, 96928–96933, doi:10.1039/C5RA18679J.
32. Ghediya, P.R.; Joshi, K.K.; Kasela, P.A.; Chaudhuri, T.K.; Kandoliya, M. Effect of solvents on physical properties of direct-coated Cu2CoSnS4 films. *Mater. Res. Express* **2019**, *6*, 106419, doi:10.1088/2053-1591/ab3ae5.
33. Mokurala, K.; Mallick, S.; Bhargava, P.; Siol, S.; Klein, T.R.; van Hest, M.F.A.M. Influence of dipping cycles on physical, optical, and electrical properties of Cu2NiSnS4: Direct solution dip coating for photovoltaic applications. *J. Alloys Compd.* **2017**, *725*, 510–518, doi:10.1016/j.jallcom.2017.07.188.
34. Luo, Y.-S.; Zhang, W.-D.; Dai, X.-J.; Yang, Y.; Fu, S.-Y. Facile Synthesis and Luminescent Properties of Novel Flowerlike BaMoO4 Nanostructures by a Simple Hydrothermal Route. *J. Phys. Chem. C* **2009**, *113*, 4856–4861, doi:10.1021/jp811038f.
35. Shadrokh, Z.; Eshghi, H.; Yazdani, A. Investigating the effects of temperature and metal ion ratio on physical and optical properties of Cu2ZnSnS4 nanoparticles and thin films. *Mater. Sci. Semicond. Process.* **2015**, *40*, 752–758, doi:10.1016/j.mssp.2015.06.082.

36. Zhou, Y.-L.; Zhou, W.-H.; Li, M.; Du, Y.-F.; Wu, S.-X. Hierarchical Cu2ZnSnS4 Particles for a Low-Cost Solar Cell: Morphology Control and Growth Mechanism. *J. Phys. Chem. C* **2011**, *115*, 19632–19639, doi:10.1021/jp206728b.
37. Cui, Y.; Deng, R.; Wang, G.; Pan, D. A general strategy for synthesis of quaternary semiconductor Cu2MSnS4 (M = Co2+, Fe2+, Ni2+, Mn2+) nanocrystals. *J. Mater. Chem.* **2012**, *22*, 23136–23140, doi:10.1039/C2JM33574C.
38. Ghosh, A.; Chaudhary, D.K.; Biswas, A.; Thangavel, R.; Udayabhanu, G. Solution-processed Cu2XSnS4 (X = Fe, Co, Ni) photo-electrochemical and thin film solar cells on vertically grown ZnO nanorod arrays. *RSC Adv.* **2016**, *6*, 115204–115212, doi:10.1039/C6RA24149B.
39. Ozel, F.; Aslan, E.; Istanbullu, B.; Akay, O.; Hatay Patir, I. Photocatalytic hydrogen evolution based on Cu2ZnSnS4, Cu2NiSnS4 and Cu2CoSnS4 nanocrystals. *Appl. Catal. B Environ.* **2016**, *198*, 67–73, doi:10.1016/j.apcatb.2016.05.053.
40. Chihi, A.; Boujmil, M.F.; Bessais, B. Synthesis and characterization of photoactive material Cu2NiSnS4 thin films. *J. Mater. Sci. Mater. Electron.* **2019**, *30*, 3338–3348, doi:10.1007/s10854-018-00607-z.
41. Behrouznejad, F.; Shahbazi, S.; Taghavinia, N.; Wu, H.-P.; Diau, E.W.-G. A study on utilizing different metals as the back contact of CH3NH3PbI3 perovskite solar cells. *J. Mater. Chem. A* **2016**, *4*, 13488–13498, doi:10.1039/C6TA05938D.
42. Wei, Z.; Chen, H.; Yan, K.; Zheng, X.; Yang, S. Hysteresis-free multi-walled carbon nanotube-based perovskite solar cells with a high fill factor. *J. Mater. Chem. A* **2015**, *3*, 24226–24231, doi:10.1039/C5TA07714A.
43. Chen, B.; Yang, M.; Priya, S.; Zhu, K. Origin of J–V Hysteresis in Perovskite Solar Cells. *J. Phys. Chem. Lett.* **2016**, *7*, 905–917, doi:10.1021/acs.jpclett.6b00215.
44. Dhawale, D.S.; Ali, A.; Lokhande, A.C. Impact of various dopant elements on the properties of kesterite. compounds for solar cell application: A status review. *Sustain. Energy Fuels* **2019**, *3*, 1365–1383, doi:10.1039/C9SE00040B.